PNAS RESEARCH ARTICLE | NEUROSCIENCE

Single-neuron bursts encode pathological oscillations in subcortical nuclei of patients with Parkinson's disease and essential tremor

Maximilian Scherer[a], Leon A. Steiner[a,b,c], Suneil K. Kalia[a,d,e,f], Mojgan Hodaie[a,d,f,g], Andrea A. Kühn[b], Andres M. Lozano[a,d,f,g], William D. Hutchison[a,f,h], and Luka Milosevic[a,e,f,g,i,1]

Edited by György Buzsáki, New York University Grossman School of Medicine, New York, NY; received April 9, 2022; accepted July 26, 2022

Deep brain stimulation procedures offer an invaluable opportunity to study disease through intracranial recordings from awake patients. Here, we address the relationship between single-neuron and aggregate-level (local field potential; LFP) activities in the subthalamic nucleus (STN) and thalamic ventral intermediate nucleus (Vim) of patients with Parkinson's disease ($n = 19$) and essential tremor ($n = 16$), respectively. Both disorders have been characterized by pathologically elevated LFP oscillations, as well as an increased tendency for neuronal bursting. Our findings suggest that periodic single-neuron bursts encode both pathophysiological beta (13 to 33 Hz; STN) and tremor (4 to 10 Hz; Vim) LFP oscillations, evidenced by strong time-frequency and phase-coupling relationships between the bursting and LFP signals. Spiking activity occurring outside of bursts had no relationship to the LFP. In STN, bursting activity most commonly preceded the LFP oscillation, suggesting that neuronal bursting generated within STN may give rise to an aggregate-level LFP oscillation. In Vim, LFP oscillations most commonly preceded bursting activity, suggesting that neuronal firing may be entrained by periodic afferent inputs. In both STN and Vim, the phase-coupling relationship between LFP and high-frequency oscillation (HFO) signals closely resembled the relationships between the LFP and single-neuron bursting. This suggests that periodic single-neuron bursting is likely representative of a higher spatial and temporal resolution readout of periodic increases in the amplitude of HFOs, which themselves may be a higher resolution readout of aggregate-level LFP oscillations. Overall, our results may reconcile "rate" and "oscillation" models of Parkinson's disease and shed light on the single-neuron basis and origin of pathophysiological oscillations in movement disorders.

subthalamic nucleus | ventral intermediate thalamus | single neurons | local field potentials | movement disorders

Significance

Leveraging intracranial recordings from patients with Parkinson's disease and essential tremor, the applied analyses allowed for derivation of relationships between neural signals across spatiotemporal resolutions, techniques that may facilitate interpretation of aggregate-level oscillations in various neuroscientific contexts from the perspective of the single-neuron resolution. Of relevance in Parkinson's disease, the applied methodologies allowed us to establish a link between single-neuron bursting and elevated local field potential (LFP) activities, reconciling parallel theories of neurocircuit dysfunction. Directional connectivity analyses between single-neuron and LFP signals furthermore allowed us to speculate on the origin of beta and tremor-related oscillations associated with Parkinson's disease and essential tremor, respectively. Ultimately, our findings may aid in developing targeted neurotherapeutics to address aberrant pattens of neural activity.

The symptoms of Parkinson's disease (akinetic-rigid features) and essential tremor are associated with pathologically elevated local field potential (LFP) activity in the subthalamic nucleus (STN; beta frequency oscillations; 13 to 33 Hz) and the thalamic ventral intermediate nucleus (Vim; tremor frequency oscillations; 4 to 10 Hz), respectively (1, 2). Moreover, both of these disorders have been associated with dysregulated patterns of action potential firing at single-neuron resolution. Extracellular microelectrodes acquired during neurosurgery, as leveraged in this work, enable the simultaneous acquisition of single-neuron and aggregate neuronal (LFP) signals. LFPs are generally perceived as conglomerate neural activity, with contributions from action potential firing and subthreshold transmembrane currents; however, spiking activity traditionally has not been thought to substantially contribute to periodic oscillations in the LFP (3, 4) due to the short time course of spiking signals and general sparsity of synchronous firing under physiological conditions (5). In Parkinson's disease, this conceptual disconnect has contributed to the development of parallel theories of circuit dysfunction and information coding, differentially focusing on "rate" versus "oscillation" changes to explain the emergence of symptoms. In fact, recent attempts in establishing relationships between the firing rates of individual neurons and the amplitude of beta oscillations in the healthy macaque motor cortex have been unsuccessful (6). Here, we hypothesize that periodic hypersynchronous neuronal bursting is representative of a corroborative link between competing theories. We leverage signal processing techniques to derive relationships between brain signals across spatiotemporal resolutions, which allowed us to speculate on the neuronal origin of the aforementioned pathophysiological oscillations.

Indeed, beta frequency LFPs within the dorsolateral STN have been shown to correlate with clinical symptoms (7); however, studies in animal models of Parkinson's disease have also suggested that pathological phenotypes can be dissociated from beta

This article is a PNAS Direct Submission.

[1]To whom correspondence may be addressed. Email: luka.milosevic@mail.utoronto.ca.

This article contains supporting information online at http://www.pnas.org/lookup/suppl/doi:10.1073/pnas.2205881119/-/DCSupplemental.

Published August 26, 2022.

oscillations (8, 9). Instead, it was shown that functional impairment could be exclusively controlled by burst-firing patterns of the STN (8). Thus, the relationship between the STN LFP and somatic firing remains contentious (9). At the single-neuron resolution, STN neurons exhibit increased firing rates and a strong tendency to fire in bursts (10, 11). Most recently, STN neurons that display burst firing patterns have been shown to represent a distinct neuronal population that, much like the source of STN beta oscillations, cluster in the dorsolateral STN (12, 13). Despite this topographical overlap, a relationship between neuronal bursting and LFP oscillations has not yet been characterized.

Electrophysiological studies have moreover demonstrated tremor-related LFP clusters in Vim (14), as well as tremor-related single-neuron bursting that is congruent with peripheral tremor (2, 15). However, mechanisms underlying the emergence of pathophysiological tremor-frequency oscillations have been elusive. Postmortem studies have described various levels of cerebellar degeneration in patients with essential tremor (16), including lower levels of GABAergic tone (17). While lower inhibitory tone may contribute to increased disinhibition of deep cerebellar neurons, it does not explain the emergence of a periodic oscillation. However, a recent optogenetics study has suggested that synaptic pruning deficits of climbing fiber to Purkinje cell synapses may give rise to an increased propensity for cerebellar oscillations (18), which may subsequently spread throughout the cerebello-thalamo-cortical circuit.

Here, we address the relationship between LFP and single-neuron activity in the STN and Vim of surgical patients using frequency, time-frequency, and phase-amplitude coupling (PAC; i.e., functional connectivity) analyses. As neurons are capable of multiplexing (19), and as neuronal bursting (20) appears to represent a pathophysiological hallmark in both Parkinson's disease and essential tremor, single-neuron activity was separated into bursting and nonbursting episodes throughout the analyses. We moreover examined the temporal sequence between bursting and LFP activities using effective connectivity (i.e., directionality) analyses to investigate whether periodic bursting may give rise to aggregate-level (LFP) oscillations, or whether the oscillation may in fact entrain neuronal firing, enabling us to speculate on the origin of these deleterious oscillations. Ultimately, we aimed to provide insights as to whether the interaction between spiking activity and LFP conforms to a singular principle or whether this relationship needs to be investigated separately across different disease-relevant nodes and frequency bands.

Results

STN Beta Spectral Power in LFP and Spiking Signals. Power spectral density (PSD) calculations were used to investigate beta peaks in the LFP signals, as seen in Fig. 1 *B* and *C*. PSD calculations performed on enveloped spiking activity revealed that the major contributor to the PSD peak was neuronal bursting (e.g., Fig. 1*B*). Increased PAC coincided with simultaneously increased LFP and spiking activity power levels during bursts ($P = 6e{-}11$; Fig. 1*D*, *i*), indicative of strong temporal overlap between periodic single-neuron bursting and elevated beta power in the LFP. However, this temporal overlap was also present during nonbursting activity ($P = 0.014$; Fig. 1*D*, *ii*) although to a much lesser degree. We were moreover interested to investigate whether potential relationships existed between spike firing characteristics and PSD calculations. We found a greater percentage of spikes within bursts for strong compared to weak beta neurons ($P = 6e{-}11$; Fig. 1*D*, *iii*), and that the average firing rate was greater for strong compared to weak beta neurons ($P = 9e{-}5$; Fig. 1*D*, *iv*) (for details regarding the classification of strong versus weak beta, please refer to the *Materials and Methods* section "*Spectral Power in LFP and Spiking Signals*"). We moreover found a significant relationship between STN spike firing rate and oscillatory information carried within the spike train (i.e., PSD calculations performed on enveloped spiking signal; $P = 0.004$; Fig. 1*D*, *v*).

Functional Connectivity between STN Beta LFP and Spike Signals. PAC analyses were performed to establish whether spiking activity was confined to a particular phase of the LFP oscillation. The highest PAC score was found for burst-thresholded spiking classified as having strong beta (Fig. 2*A*). In particular, the PAC scores for strong beta burst-thresholded spiking were higher than the PAC scores for strong beta nonburst-thresholded ($P = 3e{-}6$), weak beta burst-thresholded ($P = 3e{-}11$), and weak beta nonburst-thresholded ($P = 9e{-}12$) spiking.

Although it was revealed that strong beta burst-thresholded spiking had the highest PAC with the LFP signal, a sinusoidal shape was nevertheless present for strong beta nonburst-thresholded spiking (Fig. 2*A*). We hypothesized that this relationship may have been driven by high-frequency oscillation (HFO) activity contained within the spiking signals, which has been suggested to be representative of low-amplitude multiunit spiking activity, or neuronal noise. After separating HFO components (Fig. 2*B*), strong beta burst-thresholded spiking with HFO removed showed a stronger PAC relationship than strong beta nonburst-thresholded spiking with HFO removed ($P = 2e{-}7$) and HFO alone ($P = 3e{-}6$). Notably, uniform PAC from nonburst-thresholded spiking was absent upon removal of the HFO but preserved within the HFO-only signal.

Effective Connectivity between STN Beta LFP and Spike Signals. Having identified that the most robust relationship between spiking and LFP activity was during periods of single-neuron bursting (when the HFO was removed), we subsequently analyzed the directional information flow between the strong beta burst-thresholded spiking with HFO removed and the LFP signal (Fig. 2*C*). This revealed that bursting activity preceded LFP activity in 64% of recordings, while bursting succeeded LFP activity in 36% of recordings. We looked at PAC relationships once more after categorizing data by temporal sequence. While the shape of the PAC curve was more uniform for bursts preceding the LFP, the difference in PAC scores was not significant between preceding versus succeeding bursts ($P = 0.844$). Finally, preceding bursts expressed a clear sinusoidal distribution with a $\sim -110°$ phase preference.

Vim Tremor-Band Spectral Power in LFP and Spiking Signals. As with STN beta, neuronal bursting was a major contributor to the Vim tremor-related power spectrum (e.g., Fig. 3*B*). Increased PAC coincided with simultaneously increased LFP and spiking activity power levels only during bursts ($P = 0.004$; Fig. 3*D*, *i*) and not during nonbursting activity (where no PAC was present; thus, a statistic could not be calculated; Fig. 3*D*, *ii*). We moreover found a greater percentage of spikes within bursts for strong compared to weak tremor neurons ($P = 0$; Fig. 3*D*, *iii*) but no significant difference in the firing rate between strong and weak tremor neurons ($P = 0.721$; Fig. 3*D*, *iv*). Moreover, we did not find a significant relationship between the Vim spike firing rate and oscillatory information carried within the spike train (i.e., PSD calculations performed on the unthresholded enveloped spiking power; $P = 0.123$; Fig. 3*D*, *v*).

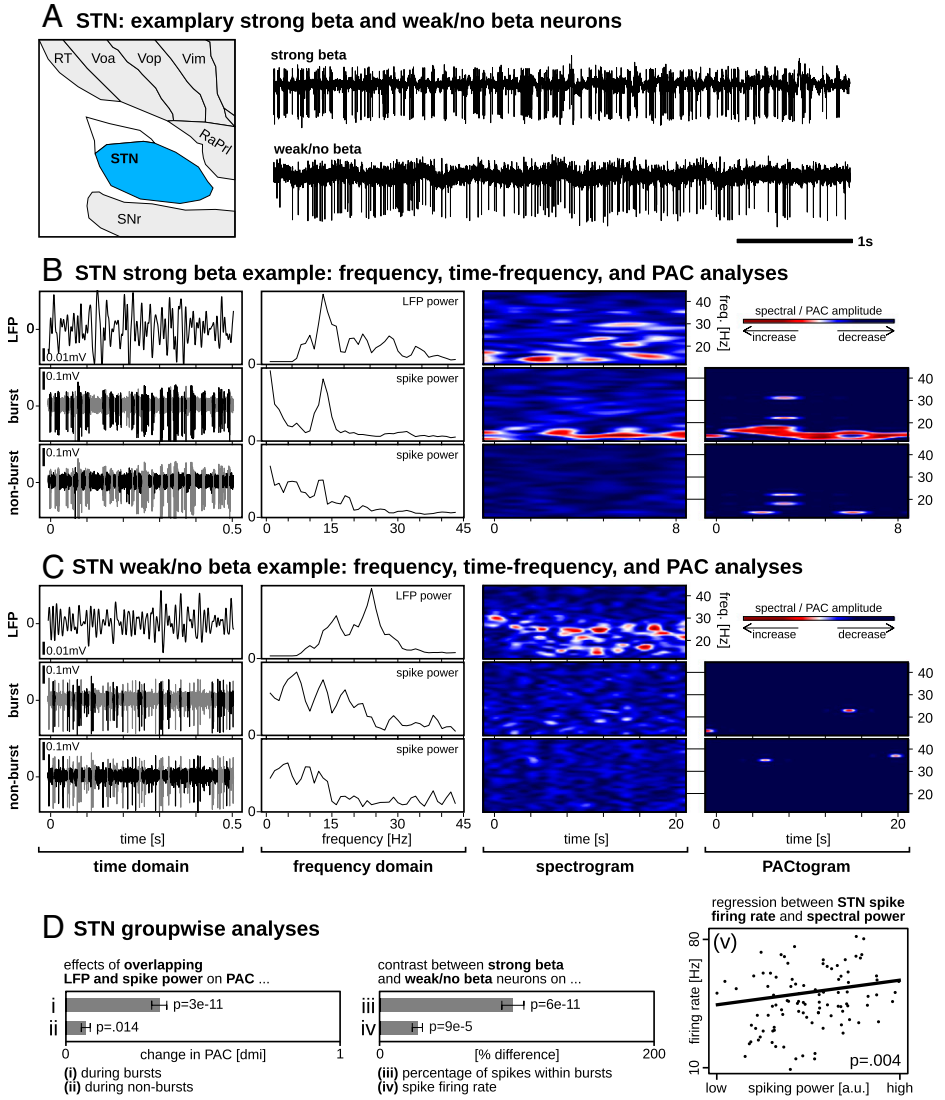

Fig. 1. STN single-neuron and LFP activities. (*A*) Exemplary strong beta neuron showing periodic neuronal bursting and a weak/no-beta neuron with minimal bursting. (*B* and *C*) Raw traces are divided into LFP, burst-thresholded, and nonburst-thresholded signal components. From left to right: same sample data as in (*A*), but at a higher time resolution; PSD estimates showing prominent frequency-matched peaks for LFP and burst-thresholded signals only; time-frequency spectrograms showing prominent frequency-matched oscillations for LFP and burst-thresholded signals only; PACtogram showing the strength of PAC over time between the LFP and corresponding single-neuron signals. (*D*) Group-wise statistics showing that significantly increased PAC coincided with simultaneously increased LFP and spike PSD power (*i*) during bursts and (*ii*) during nonbursting activity, although to a much lesser degree; (*iii*) the percentage of spikes within bursts and (*iv*) firing rates were significantly greater for strong compared to weak beta neurons; (*v*) there was a significant relationship between STN spike firing rate and PSD calculations performed on unthresholded spiking signal.

Functional Connectivity between Vim Tremor-Band LFP and Spike Signals. As with STN, the highest PAC score was found for strong tremor burst-thresholded spiking (Fig. 4*A*). In particular, PAC scores of strong tremor burst-thresholded spiking were higher than the PAC scores of strong tremor nonburst-thresholded ($P = 2e{-}5$), weak tremor burst-thresholded ($P = 9e{-}20$), and weak tremor nonburst-thresholded ($P = 7e{-}15$) spiking.

HFO separation (Fig. 4*B*) revealed that strong beta burst-thresholded spiking with HFO removed was associated with a stronger PAC than strong beta nonburst thresholded spiking with HFO removed ($P = 2e{-}7$) and HFO alone ($P = 0.003$).

Effective Connectivity between Vim Tremor-Related LFP and Spike Signals. Directionality analyses (Fig. 4*C*) revealed that strong tremor burst-thresholded spiking with HFO removed preceded LFP activity in 35% of recordings, whereas bursting succeeded LFP activity in 65% of recordings. This preferred temporal sequence was opposite to our observation for STN beta. We moreover found a small but not statistically significant ($P = 0.089$) difference in PAC score when comparing neurons succeeding versus preceding LFP activity. Finally, succeeding bursts expressed a clear sinusoidal distribution with a $\sim\pm180°$ phase preference.

Discussion

We explored the relationship between LFPs and single-neuron activity in the context of STN beta oscillations in Parkinson's disease and Vim tremor oscillations in essential tremor. Discoveries of pathophysiological changes across various spatial and temporal resolutions have led to the development of mechanistic models to explain circuit dysfunction (21). In Parkinson's disease, for example, the "rate" model suggests that changes in single-neuron rates and patterns across nodes of the basal ganglia give rise to certain clinical symptoms of the disorder. The "oscillation" model suggests that local clusters of individual neurons synchronize their

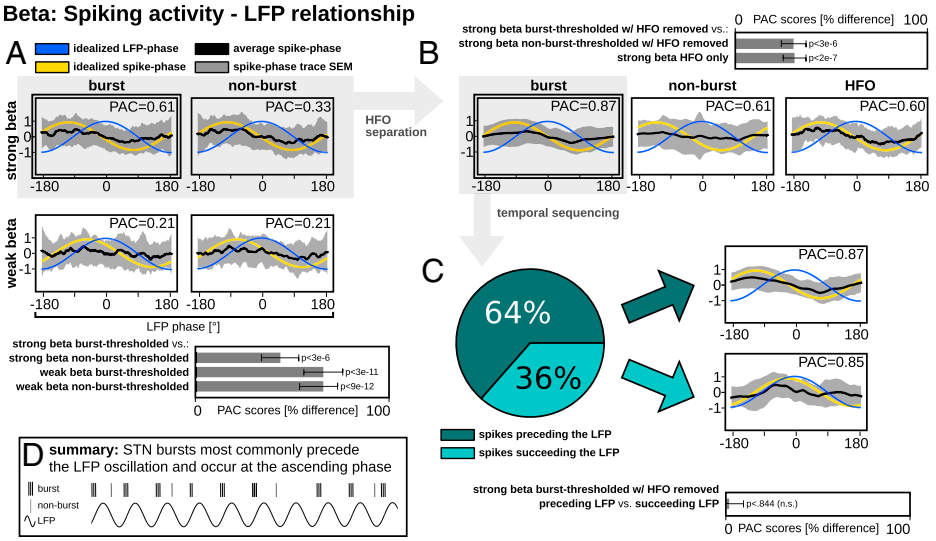

Fig. 2. Group-wise phase-coupling between beta LFP and single-neuron activities in STN. (*A*) The greatest PAC relationship was found between LFP and strong beta burst-thresholded spiking, and this relationship was significantly greater than the three other conditions. (*B*) Upon removal of the HFO from strong beta spiking signals, the PAC sinusoidality of nonburst-thresholded spiking dissipated but was preserved for burst-thresholded spiking and the HFO-only signal. PAC was significantly greater for burst-thresholded spiking with HFO removed than the two other conditions. (*C*) Based on directionality analyses, burst-thresholded spiking activity preceded the LFP oscillation 64% of the time; however, when signals were stratified by temporal sequence, PAC was not significantly different between the two conditions. (*D*) A schematic summary of the main findings.

activity, giving rise to rhythmic, pathophysiologically elevated aggregate-level oscillations. Although both models attempt to abstract pathophysiological processes of the same disorder, there has been little conceptual overlap, leading to the suggestion that these processes may be mutually exclusive (8). By exploring the relationship between single-neuron activity and aggregate-level LFP oscillations, we investigated whether rate and oscillatory neural correlates converge to a common electrophysiological signature or should be conceptualized as distinct hallmarks of the underlying pathophysiology. Overall, our results agree with previous studies that have suggested a relationship between spiking and LFP activity (22–24), but provide additional insights by identifying the critical role of neuronal bursting in facilitating this relationship across spatial and temporal resolutions.

Neural Coding with Bursts to Reconcile Rate and Oscillation Theories. We found distinct peaks within power spectral estimations performed on enveloped spiking activity that corresponded to peaks within the power spectra of LFPs (Figs. 1 and 3). However, spiking activity thresholded to contain busting only resulted in far stronger power spectral estimates, whereas spiking activity occurring outside of bursts carried almost no oscillatory information. Moreover, we found a large degree of temporal overlap between the periodic bursting of single-neuron activity and the ongoing LFP oscillation, both confined to the same frequency band (Figs. 1*D*, *i* and 3*D*, *i* and corresponding PACtograms). These findings suggest that bursting activity within the spike train may represent a high spatial resolution readout of the aggregate level LFP oscillation (discussed in more detail in the following sections). Indeed, recordings with strong beta or strong tremor oscillatory activity in the LFP had more bursting than recordings with weaker oscillatory activity (Figs. 1*D*, *iii* and 3*D*, *iii*). Moreover, the percentage of spikes within bursts was greater in Vim recordings with strong tremor-related activity than in STN recordings with strong beta ($P = 2e{-}5$; not depicted), suggesting the transient (25, 26) nature of elevated beta LFPs compared to more sustained/enduring Vim tremor-related oscillations.

Neuronal bursting is a ubiquitous physiological means of neural information coding (27), serving several important functional roles in the brain. One such role is to increase the reliability of information transfer across synapses (28). However, pervasive and highly correlated neuronal bursting in STN and Vim may represent a maladaptive change to brain circuitry that overwhelms other meaningful forms of information transfer (29). To this end, excessive STN and Vim bursting can indeed explain specific clinical features of Parkinson's disease and essential tremor, respectively.

Our findings suggest important implications of neuronal bursting activity as a means of reconciling and corroborating the "rate" (30, 31) and "oscillation" (32) models of Parkinson's disease. The rate model suggests that dopaminergic degeneration (among other sequelae) results in decreased inhibition of the STN and subsequent overexcitation of the globus pallidus internus and substantia nigra pars reticulata, which in turn overinhibit thalamocortical and brainstem motor networks, resulting in the hypokinetic symptoms of Parkinson's disease. In addition to increased firing rates, there is also an increased propensity for neuronal bursting within STN. Rather than considering individual neurons, the oscillation model implicates synchronous, aggregate-level network oscillations in the beta frequency band as a pathophysiological hallmark of the akinetic-rigid features of Parkinson's disease (7, 33–35). Within this work, we show a direct temporal link between neuronal bursting activity and the aggregate-level LFP oscillation (via PAC results), additionally corroborating the topographical overlap of these phenomena in STN (12, 13). As such, we suggest that the single-neuron rate model and LFP oscillation model, both hallmarks of the hypokinetic features of Parkinson's disease, are in fact not distinct and competing theories, but can be linked directly to one another through bursting. Our results suggest that increased beta activity in the STN LFP represents a functional readout of an increased propensity for periodic neuronal bursting (likely synchronized across many neurons), which is also associated with a net increase in neuronal output (Fig. 1*D*, *iii*–*iv*). This explanation may therefore reconcile the rate and oscillation models of Parkinson's disease (Fig. 1*D*, *v*), particularly given that both models implicate the hypokinetic features of the disorder and given that both neuronal firing rates/patterns and LFP oscillations are modulated by voluntary movements (36, 37) (*SI Appendix*, Figs. 2 and 3) and

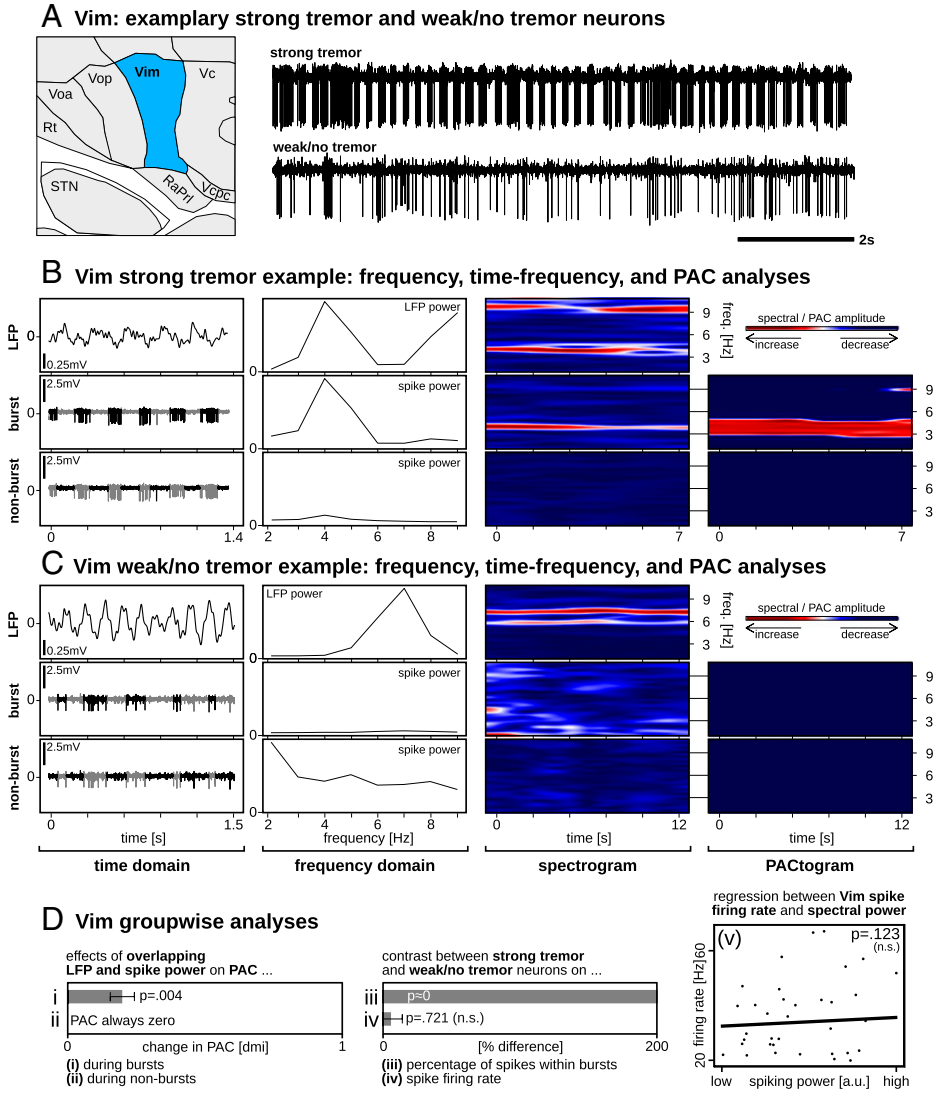

Fig. 3. Vim single-neuron and LFP activities. (*A*) Exemplary strong tremor neuron showing periodic neuronal bursting and a weak/no-tremor neuron with minimal bursting. (*B* and *C*) Raw traces are divided into LFP, burst-thresholded, and nonburst-thresholded signal components. From left to right: same sample data as in (*A*), but at a higher time resolution; PSD estimates showing prominent frequency-matched peaks for LFP and burst-thresholded signals only; time-frequency spectrograms showing prominent frequency-matched oscillations for LFP and burst-thresholded signals only; PACtogram showing the strength of PAC over time between the LFP and corresponding single-neuron signals. (*D*) Group-wise statistics showing that significantly increased PAC coincided with simultaneously increased LFP and spike PSD power (*i*) during bursts, but (*ii*) not during nonburst spiking; (*iii*) the percentage of spikes within bursts was significantly greater for strong compared to weak tremor neurons, (*iv*) but no differences were found in firing rates, (*v*) nor was there a relationship between STN spike firing rate and PSD calculations.

antiparkinsonian medications (38, 39). Moreover, therapeutic deep brain stimulation has been suggested to disrupt pathological pattens of activity (40) through LFP desynchronization (41), local suppression (42) and desynchronization of pattered firing (15), and regularization of efferent output (43). A rate model in essential tremor has not previously been put forth; however, pathophysiologically elevated tremor-related neuronal bursting in the Vim is a well-known phenomenon (2). As with STN beta activity, we established a strong link between neuronal bursting and the tremor-frequency LFP signal in the Vim. Circuit dysfunction in essential tremor is indeed characterized by an increased propensity for periodic neuronal bursting across the cerebello-thalamo-cortical motor circuit, ultimately resulting in clinical/behavioral manifestations of tremor (44).

Connectivity between Neural Signals across Spatial Resolutions. For STN, the highest degree of PAC between beta LFP and spiking activity occurred during bursting, particularly when the bursting activity preceded the LFP. Importantly, before removal of the HFO signal, a PAC relationship was nevertheless present between the beta LFP and nonburst signals (Fig. 2*A*). Recent reports have described a relationship between the phase of beta LFP signals and the amplitude of HFOs within the parkinsonian STN (23) and motor cortex (45). In our analyses, the removal of HFO components from the spiking signals completely abolished any semblance of a phase-amplitude relationship between the beta LFP and isolated nonburst spiking activity (Fig. 2*B*), while emphasizing the critical contributions of isolated single-neuron bursting activity to the beta LFP. As such, increased HFO amplitudes may indeed be driven by synchronous single-neuron bursting, and our results may thus define and corroborate micro- (single-neuron), meso- (HFO), and macro- (LFP) level representations of parkinsonian subthalamic beta oscillations across multiple scales of observation (4). Although derivation of relationships between neural signals across spatiotemporal resolutions has been considered a nontrivial task (4, 6), it has

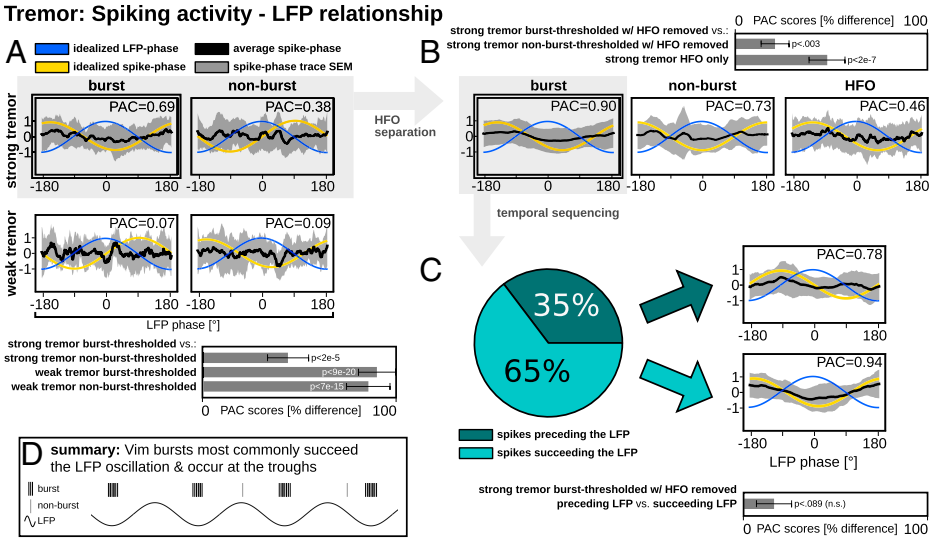

Fig. 4. Group-wise phase coupling between tremor LFP and single-neuron activities in Vim. (*A*) The greatest PAC relationship was found between LFP and strong beta burst-thresholded spiking, and this relationship was significantly greater than the three other conditions. (*B*) Removal of the HFO from strong beta spiking signals refined the sinusoidality of burst-thresholded spiking. PAC was significantly greater for burst-thresholded spiking with HFO removed than the two other conditions. (*C*) Based on directionality analyses, the LFP oscillation preceded burst-thresholded spiking activity 65% of the time; however, when signals were stratified by temporal sequence, PAC was not significantly different between the two conditions. (*D*) A schematic summary of the main findings.

indeed previously been shown in the primate motor cortex that neuronal firing rates could be directly estimated from LFP signals (46).

The above results in STN were also generally valid for tremor-related oscillations in the Vim, with three important differences: the PAC relationship was strongest when the tremor bursting in Vim succeeded LFP activity; the overall contribution of the HFO signal on nonbursting activity was less substantial; and neuronal bursting phase preference was ±180° with respect to the LFP (compared to a −110° for STN). Typically, phase preference across signals in different brain regions can be difficult to interpret, given that it may evolve over time (22) or based on medication state (38), resulting in a spectrum of phase relationships (47). However, in this work, we investigate phase relationships between signals of different spatiotemporal resolutions (i.e., spiking versus LFP) within the same structure. In the context of this work, it is possible that the difference in phase preference between STN and Vim is the result of differences in the temporal sequence/directionality between the neuronal bursting and LFP signals. To this end, our effective connectivity analysis of the temporal sequence between bursting and LFP may provide insights about the origin and propagation of pathophysiological oscillations within respective brain circuits and disorders, which are discussed in the following two sections.

On the Emergence of STN Beta Oscillations in Parkinson's Disease. Exaggerated STN beta oscillations have been correlated with clinical symptoms of Parkinson's disease (7, 34, 35). At the initiation of elevated levels of LFP oscillations, coordinated action potential firing has been observed across cortex-basal ganglia structures (22, 47). Critically, ensemble-level properties of synchronization have been shown to be underlain by the timing of action potentials in relation to cortical beta bursts, suggesting that cortical areas may be involved in the orchestration of beta activity through the basal ganglia-thalamocortical loops (22). The importance of a cortical drive is further supported by recent evidence that has shown that the hyperdirect pathway is implicated in the transduction of beta oscillations to the STN (48). Repeated observations suggest that the synchrony between cortex and STN occurs predominantly at high beta frequencies (21 to 33 Hz). However, it has been shown that low beta frequencies are more directly correlated with parkinsonian symptoms (7, 49–51). Cortical control of the STN may still be implicated in the generation of this activity, as biophysical models have revealed that an exaggerated hyperdirect pathway can lead to the generation of subcortical synchrony at lower beta frequencies (48). This suggests that the dopamine-depleted basal ganglia may provide a resonance circuit that amplifies cortical high beta, producing an exaggerated prevalence of pathological low-frequency bursts. The maintenance of subthalamic beta oscillations has been suggested to be the result of the reciprocal connections of the STN with the globus pallidus externus (47, 52). In particular, prototypic globus pallidus externus neurons have been shown to regulate beta activity by providing synaptic inhibition to STN neurons (53). When arriving in antiphase to a synchronized cortical drive (54), synaptic inhibition can support action potential generation by increasing the availability of Na^+ channels, thus promoting the precision, efficiency, and, ultimately, the synchrony of STN spiking (55). Furthermore, the STN itself has been shown to be critical for the expression of beta oscillations in 1-methyl-4-phenyl-1,2,3,6-tetrahydropyridine-treated monkeys (56, 57).

Overall, these studies implicate a role of coordinated synaptic mechanisms localized to the STN that are necessary for the generation and amplification of pathological beta oscillations. Excitatory cortical inputs to STN are thought to cause loose cortico-STN synchronization, but these excitations trigger recurrent inhibition via globus pallidus externus, which sculpts neuronal firing into the pathological beta oscillatory pattern, particularly when arriving in antiphase to the cortical inputs. It is therefore possible that this pathological oscillatory pattern is generated de novo within STN, and that elevated population-level LFP oscillations are driven by and only detectable when enough individual neurons are subject to periodic oscillations of the firing rate (i.e., it is possible that the LFP signal is a summation of synchronous action potential bursting). This would corroborate our findings that neuronal bursting most commonly precedes the LFP oscillation. Contrarily, Vim tremor-related

bursting may be the result of direct feedforward neuronal entrainment via strong periodic excitatory inputs of the cerebellum (elaborated upon below). This would corroborate our findings that neuronal bursting most commonly succeeds the LFP oscillation in Vim.

On the Emergence of Vim Tremor Oscillations. Essential tremor is regarded as a disorder of the cerebellum, evidenced by postmortem studies showing increased Purkinje cell loss (58) and axonal swelling (59) in the neocerebellum and vermis, as well as lower levels of GABA receptors in the dentate nucleus (17). However, these pathological changes do not directly explain the emergence of tremor-related oscillations. While unique ion channel dynamics in the thalamus, inferior olive, and cerebellum can generate oscillations via inhibition-induced rebound excitations (60), they have been reported to contribute to the generation of 10-Hz physiological tremor only, but not essential tremor (44). Rather, there has been an important theory that can directly explain the emergence of tremor-related oscillations based on essential tremor pathology. Recent studies in the postmortem cerebellum of patients with essential tremor have shown synaptic pruning deficits of climbing fiber to Purkinje cell synapses (61). In particular, an increased number of climbing fiber synapses on the Purkinje cell dendrites within the parallel fiber synaptic territory have been observed in essential tremor (62). These synaptic pruning deficits were linked to glutamate receptor delta 2 (GluRδ2) protein insufficiency (18). Critically, it was found that mice with GluRδ2 insufficiency and climbing fiber-to-Purkinje cell synaptic pruning deficits develop essential tremor-like behavior that could be suppressed with the viral rescue of GluRδ2 protein (18). Moreover, optogenetic or pharmacological inhibition of neuronal firing, axonal activity, or synaptic vesicle release confirmed that excessive climbing fiber-to-Purkinje cell synaptic activity was required for the generation of tremor and tremor-related oscillations in the cerebellum (18).

As such, it is likely that tremor-related oscillatory activity is generated within the cerebellum, which may subsequently spread to efferent structures, including the Vim. Strong periodic afferent inputs to Vim may therefore directly entrain local neuronal populations, which would corroborate our findings that neuronal bursting most commonly succeeds the LFP oscillation.

Limitations. There are various limitations associated with intracranial neurophysiological studies in humans, including but not limited to time constraints and the inability to use pharmacological agents or sophisticated tools such as optogenetics to elucidate ionic and molecular mechanisms of interest. However, these studies have an advantage in that it is not fully known how well animal models correspond to human conditions or anatomy. Moreover, while our connectivity results provided interesting insights regarding temporal sequence between signals, which may shed light on the origin of beta and tremor-related oscillations, the temporal sequences were not unanimous. The question of whether spiking activity drives the LFP or vice versa is in fact a ubiquitous one in neuroscience, which can only be unequivocally answered by simultaneous recording of far greater numbers of neurons than is currently feasible in humans or animals (4). Furthermore, it should be noted that a small proportion of STN neurons exhibited an antiphasic phase preference (70° versus the commonly observed −110°). Finally, in future studies, it would be valuable to assess whether differences in connectivity metrics are somatotopically organized. In this analysis, although neurons were sampled from the entire spatial extent of the STN and Vim, we do not possess information as to the precise topographic location of each sampled neuron.

Conclusions. Through the derivation of relationships between neural signals across spatiotemporal resolutions, it was found that periodic neuronal bursting encodes pathophysiological LFP oscillations in Parkinson's disease (STN beta oscillations) and essential tremor (Vim tremor-related oscillations). Increased neuronal bursting was associated with elevated LFP oscillatory power in the time, frequency, and phase domains. Overall, the findings of synchronization between periodic neuronal bursting and periods of elevated LFP oscillations may reconcile the canonical parkinsonian single-neuron rate and aggregate-level oscillation models. Furthermore, our directionality analyses allowed us to speculate on the origin of these deleterious oscillations. In STN, bursting activity most commonly preceded the LFP oscillation, suggesting that neuronal bursting generated within STN may give rise to an aggregate-level LFP oscillation. In Vim, LFP oscillations most commonly preceded bursting activity, suggesting that neuronal firing may be directly entrained by strong periodic afferent inputs. A generalizable takeaway from this work is that the applied signal-processing techniques revealed that periodic single-neuron bursting is likely representative of a higher spatiotemporal resolution readout of periodic increases in the amplitude of HFOs, which themselves are likely higher resolution readouts of aggregate-level LFP oscillations. These findings may therefore facilitate interpretation of aggregate-level oscillations, in various neuroscientific contexts, from the perspective of the single-neuron resolution and the increased propensity for patterned synchronization across local neuronal populations.

Materials and Methods

Data Acquisition. Each patient underwent deep brain stimulation implantation into the STN (akinetic-rigid dominant Parkinson's disease; $n = 19$) or VIM (essential tremor; $n = 16$). During surgery, intraoperative microelectrode recordings were used to localize STN (63) or Vim (64). Single-neuron recording segments were extracted from 117 STN neurons and 32 Vim neurons; a data overview is provided in *SI Appendix*, Table 1. Acquired electrophysiological data were sampled at ≥12.5 kHz using Guideline System GS3000 amplifiers (Axon Instruments, Union City, CA). Written informed consent was provided by all of the patients, and the study was approved by the University Health Network Research Ethics Board.

For all of the analyses described below, the same methodological techniques were applied for STN and Vim recordings; however, analyses of STN recordings were focused on beta oscillations (13 to 33 Hz), while analyses of Vim recordings were focused on tremor oscillations (4 to 10 Hz).

Extracting Individual Signals from the Superimposed Microelectrode Data. Microelectrode recording signals were divided into several individual signals throughout the analyses (S1 to S7). (S1) LFP recordings were extracted using a low-pass finite impulse response filter (50 Hz), and (S2) a high-pass finite impulse response filter (300 Hz) was used to better isolate spiking activity. Spiking activity was subsequently divided into subgroups of activity that occurred (S3) during bursts and (S4) outside of bursts (i.e., nonbursts). Burst detection was done via dissection of the interspike interval (ISI) probability distribution functions (27, 65); *SI Appendix*, Fig. 1 contains details on ISI threshold setting for beta and tremor datasets. Undesired data points in signals (S3) and (S4) were masked by either zeros for subsequent power estimates or Gaussian noise for subsequent connectivity estimates.

Spectral Power in LFP and Spiking Signals. PSD estimates (i.e., Figs. 1 and 3) were used to determine the overall amplitude of beta/tremor activity for each of the delineated signals (S1 to S4). While PSD estimations were directly calculated on the low-pass filtered LFP data (S1), spiking activity signals (S2 to S4) were first enveloped (absolute of the Hilbert transform). The PSD estimates

were calculated using Welch's (66) method (1 Hz bins, 50% overlap). PSD estimates obtained from unthresholded spiking signals (S2) were used to classify each neuron as a strong or weak beta/tremor neuron in a semiautomated manner. An initial group of strong beta/tremor neurons were identified based on visual inspection of beta/tremor peaks in the PSD plots. The remaining neurons were subsequently classified using a naive Bayes classifier trained on the manually identified samples. For the relative height of the PSD peak at beta/tremor frequency to be automatically assessable, the absolute power at the peak frequency of interest was divided by an estimate derived from the interpolation of lower and higher frequency bins surrounding the peak.

Time-frequency spectrograms were also generated from PSD estimates (beta: 2s windows, 1s window step size, and 1 Hz wide bins; tremor: 4s windows, 0.25s window step size, and 0.25 Hz wide bins). The PACtograms in Figs. 1 and 3 were generated from PAC estimates (described in detail in the following section) using 2s (beta) or 4s (tremor) data segments (beta: 1s window step size, and 1 Hz wide bins; tremor: 0.25s window step size, and 0.25 Hz wide bins) across various frequencies for the phase component of the LFP.

Functional Connectivity between LFP and Spike Signals. For PAC analyses, we leveraged the Hilbert transform to return the instantaneous amplitude and/or the instantaneous phase of a given signal (23, 45). Using these readouts, PAC plots (Figs. 2 and 4) were generated by plotting the instantaneous amplitude of burst- (S3) or nonburst- (S4) thresholded spiking signals with respect to the instantaneous phase of each cycle of the corresponding LFP signal (S1). In these plots, positive values imply spiking activity, whereas negative values imply lack of spiking. For the group-wise PAC histograms, amplitudes were normalized with respect to 25th and 75th percentiles on an individual sample level. A more sinusoidal and uniform PAC plot implies a stronger phase amplitude relationship between LFP and spiking activity. As such, an amplitude constrained (0.95 to 1.05) sinusoidal function was fit to each recorded sample individually. The resulting PAC score describes the goodness of fit between the fitted sinusoid and the sampled data points. The score was quantified as one minus the normalized mean square error between the sinusoidal fit and the generated PAC waveform. The PAC plots also enabled the determination of the average phase preference between LFP and spiking activities. The phase offset was determined by comparing the group-wise fitted sinusoidal function (yellow curves in Figs. 2 and 4) to an idealized sinusoidal function with zero phase shift (blue curves in Figs. 2 and 4).

We also took into consideration that each of the signals (S3) and (S4) (burst- and nonburst-thresholded spiking, respectively) also contained high-frequency oscillatory activity (>300 Hz) in addition to spiking activity. In general, HFOs are thought to represent aggregate spiking activity, or neuronal noise. Previous reports have suggested that HFO amplitude modulation is a representation of synchronized spiking activity across a local cluster (23). Therefore, in subsequent analyses (Figs. 2*B* and 4*B*), we removed HFO activity from the spiking signals (S3) and (S4) to generate (S5) burst-thresholded spiking with HFO removed, and (S6) nonburst-thresholded spiking with HFO removed. We also generated an (S7) HFO-only signal by removing spiking activity from the high-pass filtered signal (S2). Unwanted data points were replaced with Gaussian white noise. As only strong beta/tremor signals expressed high PAC values, the following analyses were exclusive to recordings from these neurons. As only strong beta/tremor signals expressed high PAC values, these analyses were exclusive to recordings from these neurons.

Effective Connectivity between LFP and Spike Signals. Temporal sequence between LFP and spiking activity (i.e., which signal precedes which) was determined using same-frequency connectivity estimates. These estimates were calculated from burst-thresholded spiking with HFO removed (S5) of strong beta/tremor neurons as these signals expressed a much stronger PAC than their nonburst counterparts (S6). Same-frequency coupling was estimated using directionalized absolute coherence (3° minimal angle threshold). Briefly, directionalized absolute coherence is a conglomerate same-frequency coupling metric that quantifies the direction of the information flow using the phase slope index, volume conductance via imaginary coherency, and magnitude of the relationship via magnitude squared coherence (67). Based on the results of supercritical fluid chromatography analysis, each individual recording was subdivided based on whether spiking activity preceded LFP activity or vice versa. PAC analyses were subsequently repeated on these subgroups (Figs. 2*C* and 4*C*).

Statistical Analyses. Several group-wise statistical tests were computed based on the analyses presented in Fig. 1 for STN beta and Fig. 3 for Vim tremor. We were interested in whether there were time- and frequency-dependent overlaps in the time-frequency spectrograms of LFP and spiking signals and whether these overlaps in elevated spectral power coincided with the generated PACtogram plots. To investigate this, we used the time-frequency spectrograms from LFP and enveloped spiking activity to determine areas of above-average activity. Then, we calculated the overlap between these areas across signals, and compared PAC within these areas to PAC outside these areas using linear mixed models (Figs. 1*D*, *i*/*ii* and 3*D*, *i*/*ii*). For neuronal recordings, we also used linear mixed models to assess whether there was a difference in the percentage of spikes within bursts and the average firing rate when the recording sites were stratified by oscillatory strength (i.e., strong versus weak spectral power) (Figs. 1*D*, *iii*/*iv* and 3*D*, *iii*/*iv*). Linear mixed models were also used in the context of regression analyses to determine whether relationships existed between spike firing rates and PSD calculations performed on the unthresholded spiking signals (Figs. 1*D*, *v* and 3*D*, *v*).

We also performed statistical tests using PAC scores seen in Figs. 2 and 4 by comparing each condition to the condition with the highest PAC score (i.e., reference condition). For example, in Fig. 2*A*, strong beta burst-thresholded spiking was used as a reference and PAC was compared to strong beta nonburst-thresholded, weak beta burst-thresholded, and weak beta nonburst-thresholded spiking.

For all of the linear mixed model evaluations, patient and trial identities were included as random factors to compensate for multiple measurements across and within patients. Exact linear mixed models formulas, parameters, and hypothesis counts for multiple comparison corrections (false discovery rate corrected using the Benjamini-Hochberg method (68)) are available in *SI Appendix*, Tables 2 and 3.

Data Availability. Python code is available at https://github.com/toronto-tnbs/pac_investigation and data are available at https://www.biorxiv.org/content/10.1101/2022.04.05.486956v1 (69).

ACKNOWLEDGMENTS. The authors thank the patients for their participation. This work was supported by research grants from the Natural Sciences and Engineering Council of Canada (NSERC) RGPIN-2022-05181 (to L.M.), the Alexander Von Humboldt Foundation (to M.S.), the German Research Foundation (DFG) Project-ID 424778381 TRR 295 (to L.A.S. and A.A.K.), and the Junior Clinician Scientist Program of the Berlin Institute of Health (BIH) and German Academic Exchange Service (DAAD) (to L.A.S.).

Author affiliations: [a]Krembil Brain Institute, University Health Network, Toronto, M5T 2S8, Canada; [b]Department of Neurology, Charité-Universitätsmedizin Berlin, Berlin, 10117, Germany; [c]Berlin Institute of Health (BIH), Berlin, 10178, Germany; [d]Department of Surgery, University of Toronto, Toronto, M5T 1P5, Canada; [e]KITE Research Institute, University Health Network, Toronto, M5G 2A2, Canada; [f]Center for Advancing Neurotechnological Innovation to Application (CRANIA), Toronto, M5T 2S8, Canada; [g]Institute of Medical Sciences, University of Toronto, Toronto, M5S 1A8, Canada; [h]Department of Physiology, University of Toronto, Toronto, M5S 1A8, Canada; and [i]Institute of Biomedical Engineering, University of Toronto, Toronto, M5S 3G9, Canada

Author contributions: M.S., L.A.S., and L.M. conceptualized the study and designed research; M.S. and L.M. designed the methodology; M.S., L.A.S., S.K.K., M.H., S.K.K., A.A.K., A.M.L., W.D.H., and L.M. performed research; M.H., A.A.K., A.M.L., and W.D.H. provided resources; M.S. provided the software; M.S. and L.M. curated data; M.S. and L.M. analyzed data; W.D.H. performed the validation; M.S., L.A.S., and L.M. wrote the paper; S.K.K., M.H., A.A.K., A.M.L., W.D.H., and L.M. edited the manuscript; A.A.K. and L.M. supervised the study; and L.M. acquired the funding.

Competing interest statement: Honoraria, travel funds, consultancy fees, and/or grant support have been received from Medtronic (S.K.K., M.H., A.A.K., A.M.L., W.D.H., and L.M.), Boston Scientific (S.K.K., A.A.K., and A.M.L.), St. Jude-Abbott (A.A.K. and A.M.L.), Inbrain Neuroelectronics (S.K.K.), Stada Pharm (A.A.K.), and Insightec (A.M.L.) (none of these are related to this work). M.S. and L.A.S. have no disclosures.

1. A. A. Kühn, A. Kupsch, G.-H. Schneider, P. Brown, Reduction in subthalamic 8-35 Hz oscillatory activity correlates with clinical improvement in Parkinson's disease. *Eur. J. Neurosci.* **23**, 1956–1960 (2006).
2. F. A. Lenz *et al.*, Single unit analysis of the human ventral thalamic nuclear group: Correlation of thalamic "tremor cells" with the 3-6 Hz component of parkinsonian tremor. *J. Neurosci.* **8**, 754–764 (1988).
3. P. L. Nunez, R. Srinivasan, *Electric Fields of the Brain: The Neurophysics of EEG* (Oxford University Press, New York, 2006).
4. G. Buzsáki, C. A. Anastassiou, C. Koch, The origin of extracellular fields and currents–EEG, ECoG, LFP and spikes. *Nat. Rev. Neurosci.* **13**, 407–420 (2012).
5. P. Andersen, T. V. Bliss, K. K. Skrede, Unit analysis of hippocampal polulation spikes. *Exp. Brain Res.* **13**, 208–221 (1971).

6. J. Confais, N. Malfait, T. Brochier, A. Riehle, B. E. Kilavik, Is there an intrinsic relationship between LFP beta oscillation amplitude and firing rate of individual neurons in macaque motor cortex? *Cereb. Cortex Commun.* **1**, tgaa017 (2020).
7. W.-J. Neumann *et al.*, Subthalamic synchronized oscillatory activity correlates with motor impairment in patients with Parkinson's disease. *Mov. Disord.* **31**, 1748–1751 (2016).
8. M.-K. Pan *et al.*, Neuronal firing patterns outweigh circuitry oscillations in parkinsonian motor control. *J. Clin. Invest.* **126**, 4516–4526 (2016).
9. C. B. Swan, D. J. Schulte, D. T. Brocker, W. M. Grill, Beta frequency oscillations in the subthalamic nucleus are not sufficient for the development of symptoms of parkinsonian bradykinesia/akinesia in rats. *eNeuro* **6**, ENEURO.0089-19.2019 (2019).
10. A. Benazzouz *et al.*, Intraoperative microrecordings of the subthalamic nucleus in Parkinson's disease. *Mov. Disord.* **17** (suppl. 3), S145–S149 (2002).
11. H. Bergman, T. Wichmann, B. Karmon, M. R. DeLong, The primate subthalamic nucleus. II. Neuronal activity in the MPTP model of parkinsonism. *J. Neurophysiol.* **72**, 507–520 (1994).
12. I. Tamir *et al.*, Eight cylindrical contact lead recordings in the subthalamic region localize beta oscillations source to the dorsal STN. *Neurobiol. Dis.* **146**, 105090 (2020).
13. H. Jeon *et al.*, Topographic connectivity and cellular profiling reveal detailed input pathways and functionally distinct cell types in the subthalamic nucleus. *Cell Rep.* **38**, 110439 (2022).
14. D. J. Pedrosa *et al.*, Essential tremor and tremor in Parkinson's disease are associated with distinct 'tremor clusters' in the ventral thalamus. *Exp. Neurol.* **237**, 435–443 (2012).
15. L. Milosevic *et al.*, Physiological mechanisms of thalamic ventral intermediate nucleus stimulation for tremor suppression. *Brain* **141**, 2142–2155 (2018).
16. E. D. Louis *et al.*, Neuropathological changes in essential tremor: 33 cases compared with 21 controls. *Brain* **130**, 3297–3307 (2007).
17. S. Paris-Robidas *et al.*, Defective dentate nucleus GABA receptors in essential tremor. *Brain* **135**, 105–116 (2012).
18. M.-K. Pan *et al.*, Cerebellar oscillations driven by synaptic pruning deficits of cerebellar climbing fibers contribute to tremor pathophysiology. *Sci. Transl. Med.* **12**, eaay1769 (2020).
19. M. Lankarany, D. Al-Basha, S. Ratté, S. A. Prescott, Differentially synchronized spiking enables multiplexed neural coding. *Proc. Natl. Acad. Sci. U.S.A.* **116**, 10097–10102 (2019).
20. C. Lobb, Abnormal bursting as a pathophysiological mechanism in Parkinson's disease. *Basal Ganglia* **3**, 187–195 (2014).
21. W. D. Hutchison *et al.*, Neuronal oscillations in the basal ganglia and movement disorders: Evidence from whole animal and human recordings. *J. Neurosci.* **24**, 9240–9243 (2004).
22. H. Cagnan *et al.*, Temporal evolution of beta bursts in the parkinsonian cortical and basal ganglia network. *Proc. Natl. Acad. Sci. U.S.A.* **116**, 16095–16104 (2019).
23. A. C. Meidahl *et al.*, Synchronised spiking activity underlies phase amplitude coupling in the subthalamic nucleus of Parkinson's disease patients. *Neurobiol. Dis.* **127**, 101–113 (2019).
24. A. I. Yang, N. Vanegas, C. Lungu, K. A. Zaghloul, Beta-coupled high-frequency activity and beta-locked neuronal spiking in the subthalamic nucleus of Parkinson's disease. *J. Neurosci.* **34**, 12816–12827 (2014).
25. Y. M. Kehnemouyi *et al.*, Modulation of beta bursts in subthalamic sensorimotor circuits predicts improvement in bradykinesia. *Brain* **144**, 473–486 (2021).
26. G. Tinkhauser *et al.*, Beta burst dynamics in Parkinson's disease OFF and ON dopaminergic medication. *Brain* **140**, 2968–2981 (2017).
27. F. Zeldenrust, W. J. Wadman, B. Englitz, Neural coding with bursts-current state and future perspectives. *Front. Comput. Neurosci.* **12**, 48 (2018).
28. J. E. Lisman, Bursts as a unit of neural information: Making unreliable synapses reliable. *Trends Neurosci.* **20**, 38–43 (1997).
29. H. Bergman *et al.*, Physiological aspects of information processing in the basal ganglia of normal and parkinsonian primates. *Trends Neurosci.* **21**, 32–38 (1998).
30. R. L. Albin, A. B. Young, J. B. Penney, The functional anatomy of basal ganglia disorders. *Trends Neurosci.* **12**, 366–375 (1989).
31. M. R. DeLong, Primate models of movement disorders of basal ganglia origin. *Trends Neurosci.* **13**, 281–285 (1990).
32. P. Brown, Oscillatory nature of human basal ganglia activity: Relationship to the pathophysiology of Parkinson's disease. *Mov. Disord.* **18**, 357–363 (2003).
33. C. Hammond, H. Bergman, P. Brown, Pathological synchronization in Parkinson's disease: Networks, models and treatments. *Trends Neurosci.* **30**, 357–364 (2007).
34. A. A. Kühn *et al.*, Pathological synchronisation in the subthalamic nucleus of patients with Parkinson's disease relates to both bradykinesia and rigidity. *Exp. Neurol.* **215**, 380–387 (2009).
35. L. A. Steiner *et al.*, Subthalamic beta dynamics mirror Parkinsonian bradykinesia months after neurostimulator implantation. *Mov. Disord.* **32**, 1183–1190 (2017).
36. A. Abosch, W. D. Hutchison, J. A. Saint-Cyr, J. O. Dostrovsky, A. M. Lozano, Movement-related neurons of the subthalamic nucleus in patients with Parkinson disease. *J. Neurosurg.* **97**, 1167–1172 (2002).
37. A. A. Kühn *et al.*, Event-related beta desynchronization in human subthalamic nucleus correlates with motor performance. *Brain* **127**, 735–746 (2004).
38. L. Iskhakova *et al.*, Modulation of dopamine tone induces frequency shifts in cortico-basal ganglia beta oscillations. *Nat. Commun.* **12**, 7026 (2021).
39. M. Weinberger *et al.*, Beta oscillatory activity in the subthalamic nucleus and its relation to dopaminergic response in Parkinson's disease. *J. Neurophysiol.* **96**, 3248–3256 (2006).
40. C. J. Wilson, B. Beverlin II, T. Netoff, Chaotic desynchronization as the therapeutic mechanism of deep brain stimulation. *Front. Syst. Neurosci.* **5**, 50 (2011).
41. L. K. Feldmann *et al.*, Toward therapeutic electrophysiology: Beta-band suppression as a biomarker in chronic local field potential recordings. *NPJ Parkinsons Dis.* **8**, 44 (2022).
42. L. Milosevic *et al.*, A theoretical framework for the site-specific and frequency-dependent neuronal effects of deep brain stimulation. *Brain Stimul.* **14**, 807–821 (2021).
43. Q.-X. Zhuang *et al.*, Regularizing firing patterns of rat subthalamic neurons ameliorates parkinsonian motor deficits. *J. Clin. Invest.* **128**, 5413–5427 (2018).
44. R. C. Helmich, I. Toni, G. Deuschl, B. R. Bloem, The pathophysiology of essential tremor and Parkinson's tremor. *Curr. Neurol. Neurosci. Rep.* **13**, 378 (2013).
45. C. de Hemptinne *et al.*, Exaggerated phase-amplitude coupling in the primary motor cortex in Parkinson disease. *Proc. Natl. Acad. Sci. U.S.A.* **110**, 4780–4785 (2013).
46. T. M. Hall, K. Nazarpour, A. Jackson, Real-time estimation and biofeedback of single-neuron firing rates using local field potentials. *Nat. Commun.* **5**, 5462 (2014).
47. M. D. Bevan, P. J. Magill, D. Terman, J. P. Bolam, C. J. Wilson, Move to the rhythm: Oscillations in the subthalamic nucleus-external globus pallidus network. *Trends Neurosci.* **25**, 525–531 (2002).
48. A. Oswal *et al.*, Neural signatures of hyperdirect pathway activity in Parkinson's disease. *Nat. Commun.* **12**, 5185 (2021).
49. P. Brown *et al.*, Dopamine dependency of oscillations between subthalamic nucleus and pallidum in Parkinson's disease. *J. Neurosci.* **21**, 1033–1038 (2001).
50. A. Eusebio *et al.*, Deep brain stimulation can suppress pathological synchronisation in parkinsonian patients. *J. Neurol. Neurosurg. Psychiatry* **82**, 569–573 (2011).
51. D. Whitmer *et al.*, High frequency deep brain stimulation attenuates subthalamic and cortical rhythms in Parkinson's disease. *Front. Hum. Neurosci.* **6**, 155 (2012).
52. J.-S. Brittain, P. Brown, Oscillations and the basal ganglia: Motor control and beyond. *Neuroimage* **85**, 637–647 (2014).
53. B. Crompe *et al.*, The globus pallidus orchestrates abnormal network dynamics in a model of Parkinsonism. *Nat. Commun.* **11**, 1570 (2020).
54. J. A. Goldberg *et al.*, Enhanced synchrony among primary motor cortex neurons in the 1-methyl-4-phenyl-1,2,3,6-tetrahydropyridine primate model of Parkinson's disease. *J. Neurosci.* **22**, 4639–4653 (2002).
55. J. Baufreton, J. F. Atherton, D. J. Surmeier, M. D. Bevan, Enhancement of excitatory synaptic integration by GABAergic inhibition in the subthalamic nucleus. *J. Neurosci.* **25**, 8505–8517 (2005).
56. S. Chiken, A. Nambu, Disrupting neuronal transmission: Mechanism of DBS? *Front. Syst. Neurosci.* **8**, 33 (2014).
57. Y. Tachibana, H. Iwamuro, H. Kita, M. Takada, A. Nambu, Subthalamo-pallidal interactions underlying parkinsonian neuronal oscillations in the primate basal ganglia. *Eur. J. Neurosci.* **34**, 1470–1484 (2011).
58. J. E. Axelrad *et al.*, Reduced Purkinje cell number in essential tremor: A postmortem study. *Arch. Neurol.* **65**, 101–107 (2008).
59. M. Yu *et al.*, Increased number of Purkinje cell dendritic swellings in essential tremor. *Eur. J. Neurol.* **19**, 625–630 (2012).
60. R. R. Llinás, The intrinsic electrophysiological properties of mammalian neurons: Insights into central nervous system function. *Science* **242**, 1654–1664 (1988).
61. C.-Y. Lin *et al.*, Abnormal climbing fibre-Purkinje cell synaptic connections in the essential tremor cerebellum. *Brain* **137**, 3149–3159 (2014).
62. T. Miyazaki *et al.*, Ablation of glutamate receptor GluRδ2 in adult Purkinje cells causes multiple innervation of climbing fibers by inducing aberrant invasion to parallel fiber innervation territory. *J. Neurosci.* **30**, 15196–15209 (2010).
63. W. D. Hutchison *et al.*, Neurophysiological identification of the subthalamic nucleus in surgery for Parkinson's disease. *Ann. Neurol.* **44**, 622–628 (1998).
64. I. M. Garonzik, S. E. Hua, S. Ohara, F. A. Lenz, Intraoperative microelectrode and semi-microelectrode recording during the physiological localization of the thalamic nucleus ventral intermediate. *Mov. Disord.* **17** (suppl. 3), S135–S144 (2002).
65. D. J. Bakkum *et al.*, Parameters for burst detection. *Front. Comput. Neurosci.* **7**, 193 (2014).
66. P. Welch, The use of fast Fourier transform for the estimation of power spectra: A method based on time averaging over short, modified periodograms. *IEEE Trans. Audio Electroacoust.* **15**, 70–73 (1967).
67. M. Scherer, T. Wang, R. Guggenberger, L. Milosevic, A. Gharabaghi, Directional Absolute Coherence: A phase-based measure of effective connectivity for neurophysiology data. *bioRxiv* Preprint. (2022). https://doi.org/10.1101/2022.02.07.479359 (Accessed August 10, 2022).
68. Y. Benjamini, Y. Hochberg, Controlling the false discovery rate: A practical and powerful approach to multiple testing. *J. R. Stat. Soc. B* **57**, 289–300 (1995).
69. M. Scherer *et al.*, Single-neuron bursts encode pathological oscillations in subcortical nuclei of patients with Parkinson's disease and essential tremor. bioRxiv. https://www.biorxiv.org/content/10.1101/2022.04.05.486956v1. Deposited 07 April 2022.